A Matched Dual-Tree Wavelet Denoising for Tri-Axial Swallowing Vibrations

Joshua M. Dudik * James L. Coyle † Amro El-Jaroudi Mingui Sun ‡
Ervin Sejdić

Abstract

Swallowing disorders affect thousands of patients every year. Currently utilized techniques to screen for this condition are questionably reliable and are often deployed in non-standard manners, so efforts have been put forth to generate an instrumental alternative based on cervical auscultation. These physiological signals with low signal-to-noise ratios are traditionally denoised by well-known wavelets in a discrete, single tree wavelet decomposition. We attempt to improve this widely accepted method by designing a matched wavelet for cervical auscultation signals to provide better denoising capabilities and by implementing a dual-tree complex wavelet transform to maintain time invariant properties of this filtering. We found that our matched wavelet did offer better denoising capabilities for cervical auscultation signals compared to several popular wavelets and that the dual tree complex wavelet transform did offer better time invariance when compared to the single tree structure. We conclude that this new method of denoising cervical auscultation signals could benefit applications that can spare the required computation time and complexity.

Keywords: Cervical auscultation, Wavelet denoising, Swallowing vibrations, Matched wavelets

*Joshua M. Dudik and Amro El-Jaroudi Ervin Sejdić are with Department of Electrical and Computer Engineering, Swanson School of Enginering, University of Pittsburgh, Pittsburgh, PA, USA. E-mails: jmd151@pitt.edu, amro@pitt.edu, esejdic@ieee.org. Ervin Sejdić is the corresponding author.

†James L. Coyle is with the Department of Communication Science and Disorders, School of Health and Rehabilitation Sciences, University of Pittsburgh, Pittsburgh, PA, USA. E-mail: jcoyle@pitt.edu

‡Mingui Sun is with Department of Neurological Surgery, School of Medicine, University of Pittsburgh, Pittsburgh, PA, USA. E-mail: drsun@pitt.edu.

1 Introduction

Dysphagia is a term that can be used to describe a number of swallowing disorders and impairments [1]. Though other techniques exist, the most widely utilized method of diagnosing swallowing disorders is the videofluoroscopic swallow study (VFSS) [1, 2]. For this test, a patient is asked to swallow various foods and liquids that contain a radiopaque contrast agent while observed by a trained examiner who analyzes the kinematic x-ray data for biomechanical errors and subsequent misdirection of swallowed material [3, 4]. This test is accepted as the standard diagnostic method, but it has a number of downsides. It is reliant on using a small amount of ionizing radiation, requires that the patient be able to actively participate during the exam, and assumes that the patient can travel to the examination site which could be in the same building as the patient's institutional residence or elsewhere. All of these conditions serve as potential obstacles to getting proper treatment to patients in a timely manner, thereby exposing them to prolonged risk if dysphagia is present [4–11].

To provie a more accessible method of assessment, research has been put into developing a swallowing screening technique that has both high sensitivity and specificity and can be given at a patient's bedside. Cervical auscultation, which records the sounds and vibrations made by a patient's swallow with various transducers, has been proposed as one such method [12]. Performing such an exam manually, such as with a stethoscope, has demonstrated poor accuracy and reproducibility [13–15]. However, digital transducers can not only detect signals that cannot be detected through manual analysis [12], but they also allow for mathematically processing the resulting data. Research has demonstrated that processing cervical auscultation data in this manner can improve its quality and that these signals can provide valuable information about the swallowing process, thereby increasing the accuracy of this experimental assessment method [12].

Swallowing vibrations are signals produced by numerous, temporally-overlapping physiological events that co-occur with other non-swallowing physiological events. As a result, they tend to have relatively low signal to noise ratios. Past studies have often implemented wavelet denoising techniques in order to remove much of this unwanted data [12]. However, the standard, single tree wavelet transform is time varying. Each level of the decomposition involves down sampling the input by a factor of two and causes aliasing of the signal [16]. This means that the wavelet decomposition for one swallow may be different than that corresponding to an identical swallow that was recorded only a fraction of a second later. Though the decomposition and reconstruction filters are normally balanced so as to correct for this aliasing, denoising the signal by thresholding coefficients upsets

this balance and can cause reconstruction errors. Such a situation must be accounted for, as it is impossible to precisely control the arrival time of swallowing vibration signals in a real-world situation. As a result, the single tree wavelet transform could be less effective at denoising than what may be expected while also potentially introducing new sources of errors. The dual-tree complex wavelet transform seeks to eliminate these issues caused by aliasing. In the simplest terms, it decomposes the signal with two parallel trees to create an analytical representation of the input [17]. This effectively doubles the amount of data available for analysis and allows for down sampling without aliasing [17]. This turns the wavelet decomposition into a time invariant process that maintains perfect reconstruction properties regardless of how the decomposed signal of interest is thresholded or otherwise modified [17]. While there are other methods of achieving a time-invariant denoising process, such as removing the downsampling stages entirely, the dual-tree method has a much lower computational load and does not necessarily require significant modification of the single-tree filters. Regardless, the dual-tree transform has not been previously tested with cervical auscultation data.

Wavelet denoising operates by decomposing a given signal into multiple frequency bands, eliminating any coefficients that are less than a given threshold, and then reconstructing the signal based on the remaining components [16]. The signal of interest is assumed to have a spectrum that is concentrated among a few frequencies and will produce a small number of large-amplitude components through decomposition [16]. Noise, such as Gaussian white noise, is evenly spread across all frequency bands and will produce small-amplitude components at every frequency level. The effectiveness of the thresholding step depends on the difference in amplitude between the signal components and the noise components. If the wavelet used to decompose the signal is not similar to the signal of interest, its energy will be spread across a greater number of coefficients and levels when decomposed. On the other hand, a wavelet that is well matched to the signal of interest will concentrate the signal's energy into a smaller number of coefficients, thereby maximizing the difference between the signal and noise coefficients and the effectiveness of thresholding. If a wavelet is specifically designed to have characteristics that are similar to swallowing vibrations but are dis-similar to possible noise sources, it will be easier to separate the signal components from the noise with a single threshold. As a result, it should allow for superior denoising of swallowing vibration signals when compared to more popular, generalized wavelets. Previous research into cervical auscultation signals has only utilized general wavelet families, with no attempts to optimized the wavelet shape for the given signal [12].

This manuscript investigates two key issues. First, we explore the dual-tree complex wavelet

transform and determine if this technique is useful in the context of cervical auscultation signal analysis. We suspect that the increased time-invariance of this technique will offer better denoising properties than the often used single tree decomposition. Second, this manuscript attempts to create a wavelet specifically designed to denoise cervical auscultation signals. It is assumed that using a wavelet more closely matched to the signal of interest will allow for a greater concentration of energy in fewer wavelet levels and therefore a more effective denoising process.

2 Methods

2.1 Overview

Our research utilized two set of data. The first, the artificial data set, consisted of a mathematical imitation of a swallowing signal while the second, the real data set, consisted of swallows made by healthy adults as well as adults with dysphagia. Using an existing power spectrum matching algorithm, new wavelets were created to match these two sets of signals. Using the known artificial data, the denoising effectiveness and time varying properties of both of these matched wavelets were tested against the same traits of existing, generalized wavelet families. These wavelets were implemented in both single-tree and dual-tree configurations to investigate the possible advantages of the later structure with respect to the structure that has been used in past swallowing signal research. Finally, the practical denoising effectiveness of our algorithms with respect to real swallowing signals was estimated. Again, the denoising effectiveness of both matched wavelets were compared to that provided by existing wavelet families and all wavelets were implemented in both single and dual-tree configurations. A more detailed exploration of each element of this experiment follows.

2.2 Data Sets

2.2.1 Artificial Data Set

Following the example of Sejdić et al [18], we used the following mathematical signal model to represent an artificial swallowing signal.

$$f(n) = \begin{cases} f_0(n) + 0.6\cos(210\pi nT) & 8100 \leq n \leq 16430 \\ f_0(n) + 0.5\cos(210\pi nT) & 11400 \leq n \leq 18330 \\ f_0(n) + 0.2\cos(210\pi nT) & 13200 \leq n \leq 25230 \\ f_0(n) + 0.4\cos(210\pi nT) & 12250 \leq n \leq 23400 \end{cases}$$

$$f_0(n) = 0.1\sin(8\pi nT) + 0.2\sin(2\pi nT) + 0.15\sin(20\pi nT) \\ +0.15\sin(6\pi nT) + 0.12\sin(14\pi nT) + 0.1\sin(4\pi nT) \tag{1}$$

Here, $T = 1/10000s$ and the length of the signal is 36000 samples. The resulting waveform can be seen in Figure 1. We also added Gaussian white noise to this signal with a standard deviation of 1.9 and a signal-to-noise ratio between 0.25 and 6 in increments of 0.25. This is meant to mimic the shape, duration, and frequency content of a real cervical auscultation signal, but is not derived from any real data itself. Shifted versions of this signal were created by removing up to 4200 data points in increments of 600 data points from either the leading or lagging end of the signal and placing them at the opposite side. This ensured that the overall signal energy and frequency content remained unchanged while still simulating a significant sampling delay or endpoints that are poorly aligned with the correct swallowing endpoints. A total of 1000 normal and shifted pairs were created for each signal-to-noise ratio and shift amount combination.

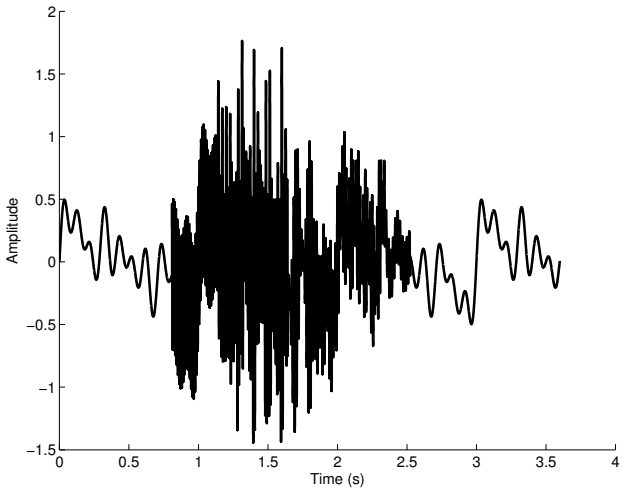

Figure 1: A mathematical imitation of a swallowing vibration signal, originally used in [18].

2.2.2 Real Data Set

Our real data consisted of swallows made by healthy adults as well as adults with dysphagia. The protocol for the study, which is described in the following passages and has been described in other published studies [19, 20], was approved by the Institutional Review Board at the University of Pittsburgh.

A total of 55 healthy participants (28 men, 27 women, mean age 39) were recruited from the neighborhoods surrounding the University of Pittsburgh campus. Each confirmed that they had

no history of swallowing disorders, head or neck trauma or major surgery, chronic smoking, or other conditions which may affect swallowing performance. The subjects were asked to complete a total of 20 independent swallows of several types of boluses (water, 'nectar' thick liquid, and 'honey' thick liquid) while their head was in a neutral position. This process was repeated with the subject's head in a 'chin-tuck' position. Five swallows of each bolus type were completed by each subject in both positions, resulting in a total of 1650 recorded swallows. The beginning and end points of each swallow were found using a custom algorithm that has been shown to provide results similar to those given by manual analysis [21].

The non-healthy participants consisted of a total of 76 patients (48 men, 28 women, mean age 63) that were scheduled to undergo a videofluoroscopic swallowing evaluation at the University of Pittsburgh Medical Center (Pittsburgh, Pennsylvania). Any patient that was scheduled for this exam was confirmed by clinical examination to have evidence of probable dysphagia or a history of swallowing difficulties. Those patients that had a history of major head or neck surgery, were equipped with assistive devices that obstructed the anterior neck such as a tracheostomy tube, or were not sufficiently competent to give informed consent were not included in the study, but no other conditions were excluded. These patients did not undergo a standardized data collection procedure, as the videofluoroscopy examination is routinely modified by the examiner to suit the individual patient. Instead, presentation order, head position, and other environmental factors were unique for each patient. The materials swallowed during the examination were of comparable consistencies (water ($<$ 5 cps), 'nectar' thick liquid ($\approx$ 300 cps),'honey' thick liquid ($\approx$ 2000 cps)) to those provided to healthy subjects based on available product information and qualitative guidelines. Included swallows were limited to those completed in either a neutral or 'chin-tuck' head position. A total of 973 swallows were recorded from these subjects. The beginning and end points were defined as the time at which the leading edge of the swallowed bolus intersected with the shadow cast on the x-ray image by the posterior border of the ramus of the mandible and the time at which the hyoid bone completed motion associated with swallowing-related pharyngeal activity and returned to its resting or pre-swallow position, respectively.

For all participants, a tri-axial accelerometer was attached to the participant's anterior neck with surgical tape. The accelerometer (ADXL 327, Analog Devices, Norwood, Massachusetts) was mounted in a custom plastic case, and affixed over the cricoid cartilage in order to provide the highest signal quality [22]. The main accelerometer axes were aligned approximately parallel to the cervical spine and perpendicular to the coronal plane and will be referred to as the superior-inferior (S-I) and anterior-posterior (A-P) axes, respectively. The third axis was perpendicular to the

others, and thereby was aligned approximately perpendicular to the sagittal plane, and is referred to as the medial-lateral (M-L) axis. The sensor was powered by a power supply (model 1504, BK Precision, Yorba Linda, California) with a 3V output, and the resulting signals were bandpass filtered from 0.1 to 3000 Hz with ten times amplification (model P55, Grass Technologies, Warwick, Rhode Island). The voltage signals for each axis of the accelerometer were both fed into a National Instruments 6210 DAQ and recorded at 20 kHz by the LabView program Signal Express (National Instruments, Austin, Texas). This setup has been proven to be effective at detecting swallowing activity in previous studies [23, 24].

Data recorded with the accelerometer underwent several processing steps to eliminate major artifacts that may complicate our denoising analysis and wavelet matching procedures. At an earlier date, the accelerometer's baseline output was recorded and modified covariance auto-regressive modelling was used to characterize the device noise [25,26]. The order of the model was determined by minimizing the Bayesian Information Criterion [25]. These autoregressive coefficients were then used to create a finite impulse response filter and whiten the recording device noise contained in our signal [25]. Afterwards, motion artefacts and other low frequency noise were removed from the signal through the use of least-square splines. As detailed in [27], a signal can be written in terms of splines as

$$x(k) = b^p(k) * c(k) \tag{2}$$

where $c(k)$ is an L_2 sequence of real numbers and $b^p(k)$ is the p^{th} order indirect spline filter, also known as a B-spline. This filter is defined as

$$b^p(k) = \frac{1}{m^n} \sum_{j=0}^{p+1} \frac{(-1)^j}{p!} \binom{p+1}{j} (k - jm)^p u(k - jm) \tag{3}$$

where u is a step function and m is a time scaling factor. It was found that, in order to minimize the mean square error of the noise approximation, $c(k)$ must be equal to (4) [27].

$$c(k) = (b^p * b^p)^{-1} * (b^p * x)(k) \tag{4}$$

In less mathematical terms, this process fits a low frequency (< 3 Hz) trend to the time domain signal that results from head motion during recording [19, 27–32]. It then subtracts that low frequency trend from the time domain recording in order to eliminate the effects of head motion without affecting the higher frequency signal [19,27–32]. In this study, we used fourth-order splines

with a number of knots equal to $\frac{Nf_l}{f_s}$, where N is the number of data points in the sample, fs is the original 20 kHz sampling frequency of our data, and the values for f_l varied with the accelerometer axis and were calculated and optimized in previous studies [27].

2.3 Dual-Tree Complex Wavelet Transform

The dual-tree complex wavelet transform has places additional requirements on the properties of its filters when compared to the single tree version. For this study, we chose to utilize the q-shift filter variant as proposed by Kingsbury [17]. In simplest terms, this filter configuration doubles the effective sampling rate of the input signal by using two filter trees with a group delay difference of one half of a sample. This results in the filters of one tree interpolating halfway between the data points analyzed by the other tree. Kingsbury recommends the easiest method of achieving this delay is to first design a single orthonormal filter pair with a group delay of one quarter of a sample [17]. One tree can then decompose the signal with the decomposition filters and reconstruct it with the time-reversed version of those filters, as is typical of the wavelet transform. The other tree uses the reconstruction filters to decompose the signal and the decomposition filters to reconstruct it, thereby adding a quarter sample delay in the opposite direction and producing an overall shift of one half of a sample. The full derivation is provided by Kingsbury in [17], but the relevant portions of their work is included here for convenience.

We first imagine a pair of discrete wavelet trees: tree a and tree b. For illustration purposes, the first two levels of the decomposition can be seen in Figure 2. Each consists of their own decomposition (H_a and H_b) and reconstruction (G_a and G_b) finite impulse response (FIR) filters. Every decomposition filter is followed by a factor of 2 downsampling stage while each reconstruction filter is preceded by a factor of 2 upsampling stage. The overall output of the system is the sum of the outputs of each wavelet tree. The response at a given decomposition level can be more simply presented the cascaded response of all higher level filters. For example, the response of wavelet tree a at the third level to a given input signal can be found by applying the third level decomposition transfer function ($H_{0a}(z)H_{00a}(z^2)H_{001a}(z^4)$) and then the third level reconstruction transfer function ($G_{001a}(z^4)G_{00a}(z^2)G_{0a}(z)$) with all other terms ignored. Here, the number of subscript digits indicates the level of the filter while a value of zero or one in the last position indicates either the scaling or wavelet filter, respectively. Naturally the same process can be applied to the second wavelet tree. If it can be shown that each level of the wavelet decomposition is shift invariant, then the same property can be assumed of the whole system.

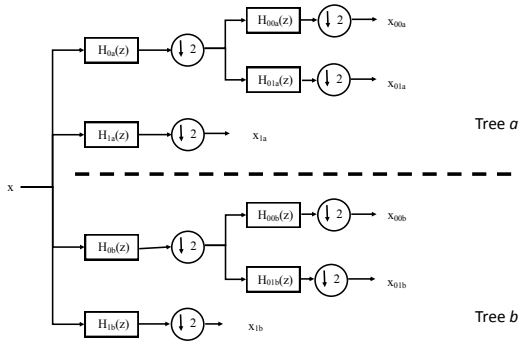

Figure 2: The first two stages of a dual-tree wavelet decomposition. The number of subscripts indicate the level of the filter, H, while the final digit indicates whether it is a scaling or wavelet filter (0 or 1, respectively). The same notation is used for the outputs of the filters. As with the single tree configuration, the reconstruction tree simply inverts this system with reconstruction filters $G(z)$.

We can define $A(z)$ and $B(z)$ as the overall decomposition transfer functions corresponding to a given decomposition level in trees a and b, respectively. Likewise, $C(z)$ and $D(z)$ can be used to represent the complementary reconstruction transfer functions. Finally, it is well known that down sampling and then up sampling a signal $U(z)$ by the same factor provides the following result:

$$V(z) = \frac{1}{M} \sum_{k=0}^{M-1} U(W^k z) \tag{5}$$

where M is the re-sampling factor and the scaling term W is equal to $e^{j2\pi/M}$. Combining these choices of notation, we can easily write the output of the dual tree system as follows:

$$Y_{overall}(z) = Y_a(z) + Y_b(z) = \frac{1}{M} \sum_{k=0}^{M-1} X(W^k z)[A(W^k z)C(z) + B(W^k z)D(z)] \tag{6}$$

where $Y_{a/b}$ is the output of the respective wavelet tree, X is the system input, and all other terms are defined. We see then, that for $k = 0$, the system behaves as expected with $W^k = 1$. However, for non-zero values of k there is potentially a non-zero response. Small values of k result in significant overlap of the frequency responses of the decomposition and reconstruction filters. This indicates aliasing of the signal and results in time-varying properties. There are two possible ways to correct for this issue. First, if the alias terms $A(W^k z)C(z)$ and $B(W^k z)D(z)$ can be made sufficiently

small, the overall system can be made approximately time invariant. In situations where this is not possible or is too difficult, such as when the filters have less than ideal transition bandwidths, the alias terms can be designed to negate each other.

For values of k greater than or equal to 2, the aliasing terms of our scaling functions can be made insignificant. The additional amount of shift in the frequency domain ensures a minimal amount of overlap between the passbands of the decomposition and reconstruction filters for most filter designs. However, this is not true when $k = 1$ and so we must design our system so that these aliasing terms cancel one another for odd k values.

$$(-1)^k A(W^k z)C(z) = B(W^k z)D(z) \tag{7}$$

A valid solution to this system can be found if the following relations are held.

$$B(z) = z^{\pm M/2}A(z) \text{ and } D(z) = z^{\mp M/2}C(z) \tag{8}$$

Observing the frequency response of the complementary wavelet filters, we can show that non-zero values of k introduce aliasing terms, as expected. However, these terms are brought about by the overlap of opposite frequency passbands. That is to say, that the positive frequency component of the unshifted filter, $C(z)$ or $D(z)$, will partially overlap with the negative frequency component of the shifted filter, $A(W^k z)$ or $B(W^k z)$, or vice versa. This suggests that the aliasing terms that occur due to the shifted wavelet filters can be cancelled by reversing the positive and negative passband polarities in one of the wavelet trees. If we define $P(z)$ and $Q(z)$ as the positive passbands of the wavelet filters of $A(z)$ and $C(z)$ and the conjugates of $P(z)$ and $Q(z)$ as the negative passbands, our dual tree system can be described as follows

$$\begin{aligned} A(z) &= 2Real[P(z)] = P(z) + P*(z) \\ B(z) &= 2Imag[P(z)] = j[P(z) - P*(z)] \\ C(z) &= 2Real[Q(z)] = Q(z) + Q*(z) \\ D(z) &= -2Imag[Q(z)] = -j[Q(z) - Q*(z)] \end{aligned} \tag{9}$$

In this form, we see that the wavelet filters of $B(z)$ and $D(z)$ are the Hilbert transforms of those in $A(z)$ and $C(z)$. When utilized in the dual-tree structure, they can be thought of as the real and imaginary parts of the system's response to an input signal. This analytic representation results in an overall system that has only a positive frequency response, resulting in half of the effective bandwidth of the single tree structure, and is approximately time invariant.

2.4 Filter Design

There are several valid designs for these sets of filters. For this project, we have chosen to utilize Kingsbury's q-shift filter relations [17]. The dual set of orthonormal wavelet filters can be calculated from a single, even-length, lowpass filter with a quarter sample group delay $H_L(z)$ as follows [17]

$$\begin{aligned} H_{00a} &= z^{-1}H_L(z^{-1}) \\ H_{01a} &= H_L(-z) \\ H_{00b} &= H_L(z) \\ H_{01b} &= z^{-1}H_L(-z^{-1}) \end{aligned} \tag{10}$$

These equations ensure that the two decomposition trees allow for perfect reconstruction of the original signal while orthogonal relationships are maintained between both the scaling and wavelet filters of each tree as well as between the filters of each individual tree. The quarter sample group delay of the scaling filter ensures that its conjugate will have a delay of three quarter samples, thereby resulting in a net half sample delay between the responses of each decomposition tree as necessary. Rather than utilize Kingsbury's method of designing this filter, we chose to create a new wavelet that is optimized for use with cervical auscultation signals.

2.5 Wavelet Matching

We followed the procedure outlined by Chapa and Rao to create a wavelet matched to a cervical auscultation signal [33]. Rather than attempting to create multiple wavelets for specific conditions, we attempted to create a generalized wavelet that would be useful for all cervical auscultation applications by matching the wavelet spectrum to the average frequency spectrum of swallowing vibrations. The procedure for obtaining individual swallow vibrations was described in section 2.2.2. Each filtered signal's spectrum was calculated using Matlab's built-in FFT algorithm and the average swallowing vibration spectrum was calculated. This spectrum was smoothed by using a weighted linear least squares method of linear regression with a window size of 50 Hz (2.5% of the signal length) so as to minimize the later amplitude matching error.

With this ideal amplitude spectrum for a swallowing wavelet, we then followed Chapa and Rao's work [33] to create a proper matched wavelet. As with the dual-tree wavelet transform, we reproduce the relevant portions of the original work [33] here for convenience.

While creating a matched wavelet function is relatively simple, ensuring that the corresponding matched scaling function maintains the requirements of an orthonormal multi-resolution analysis

is more difficult. Utilizing the well known frequency representation of the wavelet and scaling functions

$$\begin{aligned}\Phi(\omega) &= H(\frac{\omega}{2})\Phi(\frac{\omega}{2}) \\ \Psi(\omega) &= G(\frac{\omega}{2})\Psi(\frac{\omega}{2})\end{aligned} \tag{11}$$

as well as the similarly well-defined requirements of the conjugate quadrature filters $H(\omega)$ and $G(\omega)$

$$|H(\omega)|^2 + |G(\omega)|^2 = 1 \tag{12}$$

$$H(\omega)\overline{H(\omega+\pi)} + G(\omega)\overline{G(\omega+\pi)} = 0 \tag{13}$$

we can show that the scaling function power spectrum can be computed as follows.

$$|\Phi(\omega)|^2 = |\Psi(2\omega)|^2 + |\Phi(2\omega)|^2 \tag{14}$$

As is typical, Φ represents the scaling function spectrum, Ψ represents the wavelet function spectrum, and ω is the frequency. Generalizing this expression for a wavelet that is infinitely differentiable produces the following non-recursive expression.

$$|\Phi(\omega)|^2 = \sum_{j=1}^{\infty} |\Psi(2^j\omega)|^2 \tag{15}$$

This demonstrates that we can create a wavelet amplitude spectrum which matches our signal of interest and then calculate the corresponding scaling amplitude spectrum while maintaining the requirements of a multi-resolution analysis. Substituting equation 15 into the well known Poisson summation of the scaling function

$$\sum_{m=-\infty}^{\infty} |\Phi(\omega + 2\pi m)|^2 = 1 \tag{16}$$

to produce the following equation

$$\sum_{p=0}^{l} \sum_{m=-\infty}^{\infty} Y(\frac{2^l}{2^p}(k + 2^{l+1}m)) = 1 \tag{17}$$

where k is simply the discrete sample number. The absolute value of the argument of Y is bounded by the passband of our signal of interest. For this paper, we utilize a passband of $[\frac{2\pi}{3}\frac{8\pi}{3}]$ radians, which matches the passband of the common Meyer wavelet and is used by Chapa and Rao for the remainder of their work [33]. l is a defined by the sample rate of the signal of interest $\delta\omega = 2\pi/2^l$

and is equal to 4 for our work. Expanding the summations in equation 17, keeping in mind the bounds on the argument, results in the following matrix forms.

$$\sum_{i=1}^{L} a_{ik} Y(k) \tag{18}$$

$$AY = 1 \tag{19}$$

L is the number of unique samples in the passband between the lower bound and the Nyquist rate, π, and A has dimensions of Lx2^l. Naturally, both a and A can only have values of 0, 1, or 2 depending on how many valid terms can be found for the argument of Y in equation 17 for a given value of k. This matrix A is then used to build a matched wavelet spectrum from a given signal.

We define W as the sampled power spectrum of the target signal with a passband of $[\frac{2\pi}{3}\frac{8\pi}{3}]$ while Y is the corresponding power spectrum of the matched wavelet. We wish to ensure that Y closely matches W in a mean squared sense.

$$error = \frac{(W - aY)^T (W - aY)}{W^T W} \tag{20}$$

We can rearrange this equation to solve for Y directly.

$$Y = \frac{1}{a} W + A^T (AA^T)^{-1} (n - \frac{1}{a} AW) \tag{21}$$

The term a is a scaling factor, which is defined as

$$a = \frac{n^T (AA^T)^{-1} AW}{n^T (AA^T)^{-1} n} \tag{22}$$

n is a vector of dimensions 1xL where each element has a singular value while A has been defined previously.

This procedure was implemented twice for our experiment. The first utilized the artificial data described in section 2.2.1 in order to create a wavelet matched to the active, 'swallowing' portion of the signal ($8100 \leq n \leq 25230$). This serves as a baseline for the performance of a wavelet matched to a known, perfectly defined signal created using this method. The second implementation utilized the real data described in section 2.2.2. This would produce a wavelet that is most closely matched to the frequency spectrum of real swallowing vibrations and should provide superior denosing performance.

We did not follow the authors' procedure for matching the phase of our wavelet since we only cared to match the amplitude to the average swallowing spectrum. Instead, we applied a simple, quarter sample phase shift to our matched scaling function amplitude spectrum. This ensured

that the wavelet would meet the sample delay requirements set forth by Kingsbury's q-shift dual-tree complex wavelet transform [17]. Inverse transforming this signal produced the time domain representation of the scaling function of our matched wavelet. From this, it is a simple task to implement a set of FIR filters corresponding to the wavelet.

2.6 Assessment with Artificial Signals

We then used our artificial data (section 2.2.1) to examine the time invariance and the denoising effectiveness of both the single tree and dual-tree wavelet decompositions. Each individual signal was decomposed to 5 levels by both the single and dual-tree decomposition trees. Soft thresholding with the optimal threshold as calculated by [18] was used for the denoising tests. In this case, the optimal threshold was found to be $\sigma\sqrt{2\log N}$, where N is the number of samples in the data set and σ, the estimated standard deviation of the noise, is defined as the median of the down-sampled wavelet coefficients divided by 0.6745 [18]. In addition to the wavelets we matched to our artificial signal and our real data, we also denoised the signal with the Meyer and 6-tap Daubechies, Coiflet, and Symlet wavelets. As our chosen wavelet matching algorithm [33] combines properties of both the Meyer and Daubechies wavelet families, we feel that these selections will provide a reasonable point of comparison for our new wavelet filter. The process was repeated for each combination of shift amount and additive noise amplitude.

Wilcoxon rank-sum tests with a significance value of 0.05 were used to assess our results. First, the time varying properties of the single and dual-tree configurations were compared. This was done by first choosing a specific shift amount and determining the percent of the total decomposition energy that changed energy levels due to the shift. A distribution of values was produced by adjusting the amplitude of the additive Gaussian noise. The resulting distribution produced via single-tree decompositions was then compared to the distribution produced by the dual-tree decompositions. The same process was used to assess the noise reduction capabilities of the two decomposition trees, but in this situation the additive noise amplitude was held constant and the signal's shift amount was varied. These results were compared with respect to the wavelet used, so that results obtained with, for example, the Meyer wavelet in a single-tree configuration were compared with the results obtained by the Meyer wavelet in the dual-tree configuration. Further statistical comparisons were made between different wavelets with respect to their noise reduction and time varying properties with the decomposition tree held constant. For example, the single-tree Meyer wavelet noise reduction performance was compared to that provided by the single-tree

Daubechies wavelet while the dual-tree versions were also compared between one another.

2.7 Assessment with Real Signals

Since the true noise content of a real swallowing signal is unknown we used an alternative method of assessing the denoising effectiveness of our algorithms. Following the example of previous studies [18], we subtracted the approximate signal-to-noise ratio of the original signal from the signal-to-error ratio, as shown in the following equation.

$$\begin{aligned} performance &= 10\log_{10}(\frac{\sigma_x^2 - \sigma_e^2}{r}) - 10\log_{10}(\frac{\sigma_x^2 - \sigma_e^2}{\sigma_e^2}) \\ &= 10\log_{10}(\frac{\sigma_e^2}{r}) \end{aligned} \tag{23}$$

The performance is calculated in decibels and indicates the degree to which the signal-to-noise ratio was improved. σ_x^2 is the observed variance of the signal while σ_e^2 is the approximate variance of the noise and is defined as the square of the median of the down-sampled wavelet coefficients divided by 0.6745. The term r is calculated as

$$r = \frac{\sigma_e^2\sqrt{2m}}{N}(\sqrt{2m} + \beta) + d_e - \sigma_e^2 + \frac{2\alpha\sigma_e}{\sqrt{N}}\sqrt{\frac{\alpha^2\sigma_e^2}{N} + d_e - (1 - \frac{m}{N})\frac{\sigma_e^2}{2}} + \frac{2\alpha^2\sigma_e^2}{N} \tag{24}$$

where N is the length of the signal, optimal values for α and β were previously calculated to be 1 and 2.5, respectively, m is the number of coefficients that had a value greater than the threshold value, and d_e is calculated as

$$d_e = \frac{1}{N}||x - \hat{f}||^2 \tag{25}$$

where x is the original signal and $\hat{f}$ is the output of the denoising algorithm.

3 Results

Figure 3 shows the output of the amplitude matching algorithm compared to the average wavelet power spectrum amplitude of real swallowing signals within our desired passband. Figure 4 displays the time domain representation of the scaling function of our real matched wavelet derived from this amplitude match.

3.1 Shift Invariance

Figures 5 and 6 present the degree to which the single and dual-tree wavelet decompositions changed when conducted with the normal and shifted versions of our artificial signal. Specifically, it presents

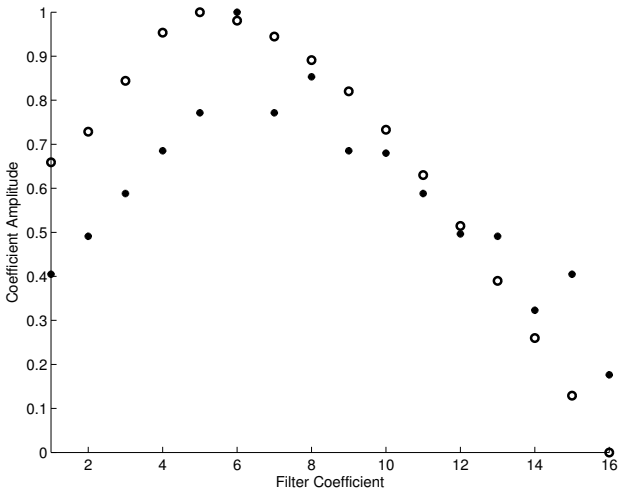

Figure 3: The open circles represent the power of our average cervical auscultation signal at discrete points within our chosen passband. The closed dots indicate the matched wavelet power spectrum as calculated by the procedure in [33].

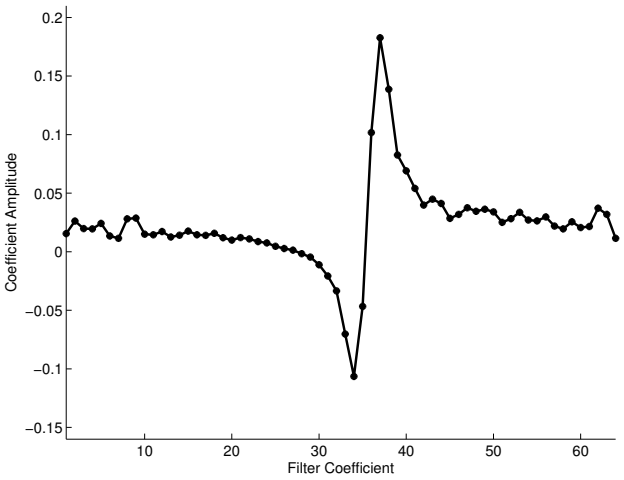

Figure 4: The scaling function derived from the matched wavelet power spectrum in 3 and the procedure described in [33].

the total amount of energy that moved between the different levels when the signal was shifted as a percentage of the total signal energy. The single and dual-tree results were shown to be significantly different $p << 0.001$, and they demonstrate that all of our wavelets possessed greater time invariant properties when used in the dual-tree system. indicating that the decomposition changed less when the input signal was shifted.

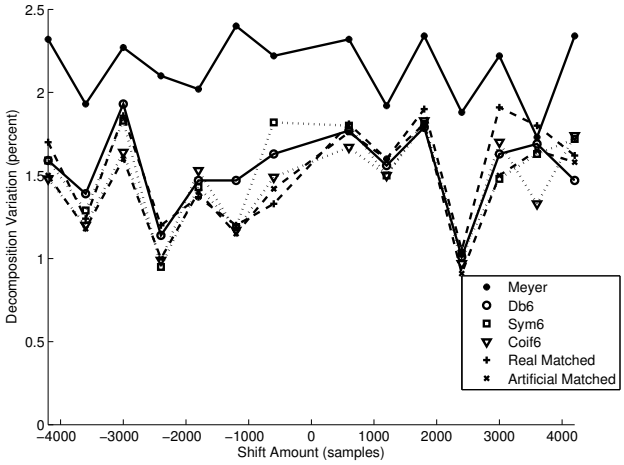

Figure 5: The percent of the signal's energy that changes decomposition levels when the artificial signal is shifted as a function of the shift magnitude. The displayed graph is for the single-tree decomposition.

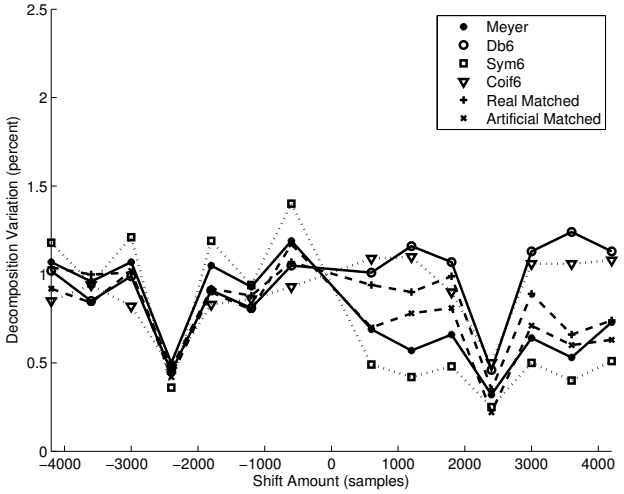

Figure 6: The percent of the signal's energy that changes decomposition levels when the artificial signal is shifted as a function of the shift magnitude. The displayed graph is for the dual-tree decomposition.

3.2 Denoising Effectiveness

Figures 7 and 8 display the signal-to-noise ratio of each denoising algorithm output as a function of the input's signal-to-noise ratio for our artificial signal. Overall, the Artificial Matched wavelet eliminated the greatest amount of noise from our artificial test signal. Comparing the single and

dual-tree implementations, we see that the Daubechies, Coiflet, and Real Matched wavelets removed a greater amount of the additive noise from the signal while the performance of the Meyer, Symlet, and Artificial Matched wavelet systems degraded to some extent when implemented in the dual-tree configuration. Again, comparing the single and dual-tree outputs resulted in statistically significant outcomes ($p << 0.001$) for all entries.

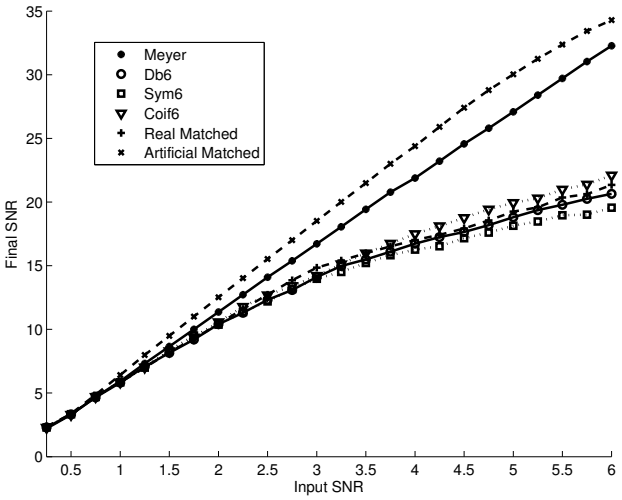

Figure 7: The output signal-to-noise ratio of the single-tree denoising algorithm as a function of the artificial input signal's signal-to-noise ratio.

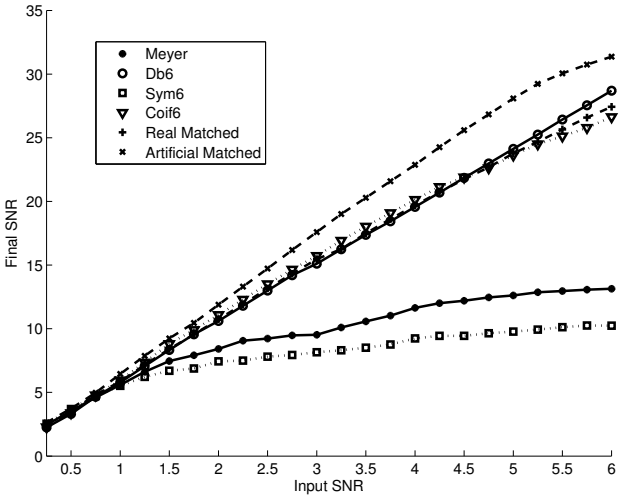

Figure 8: The output signal-to-noise ratio of the dual-tree denoising algorithm as a function of the artificial input signal's signal-to-noise ratio.

The results of our analysis with real signals is summarized in tables 1 and 2, where the relevant data is analyzed for each individual axis of vibration. We found that the Real Matched wavelet provided the best denoising ($p << 0.001$) for both the single and dual-tree configurations. We also notice that the dual-tree denoising method was able to remove a statistically greater amount of noise from the signal for all of our chosen wavelets ($p << 0.001$ for all) with the exception of the Symlet waveform.

Table 1: Single-Tree Denoising Effectiveness with Real Swallowing Signals

	Anterior-Posterior	Superior-Inferior	Medial-Lateral
Meyer	10.22 ± 1.49	10.25 ± 1.50	10.20 ± 1.49
Daubechies6	9.47 ± 1.47	9.48 ± 1.46	9.47 ± 1.46
Symlet6	9.80 ± 1.49	9.77 ± 1.50	9.79 ± 1.50
Coiflet6	8.89 ± 1.45	8.90 ± 1.44	8.89 ± 1.44
Artificial Matched	9.40 ± 1.41	9.41 ± 1.41	9.42 ± 1.40
Real Matched	10.30 ± 1.39	10.32 ± 1.40	10.29 ± 1.40

Table 2: Dual-Tree Denoising Effectiveness with Real Swallowing Signals

	Anterior-Posterior	Superior-Inferior	Medial-Lateral
Meyer	10.26 ± 0.80	10.25 ± 0.79	10.25 ± 0.79
Daubechies6	10.19 ± 0.80	10.20 ± 0.80	10.19 ± 0.79
Symlet6	9.00 ± 0.80	8.92 ± 0.79	8.96 ± 0.80
Coiflet6	10.21 ± 0.80	10.20 ± 0.80	10.20 ± 0.79
Artificial Matched	10.17 ± 0.78	10.17 ± 0.81	10.19 ± 0.80
Real Matched	10.46 ± 0.82	10.47 ± 0.82	10.46 ± 0.81

4 Discussion

4.1 Shift Invariance

In this study, we found that the dual-tree wavelet decomposition provided improved time invariant properties for all of our chosen wavelets. However, the degree of improvement varied with the wavelet, with the Meyer wavelet showing the greatest benefit when implemented in the dual-tree

system. This suggests that the dual-tree configuration provides tangible benefits for applications which use these wavelets, such as cervical auscultation. Greater time invariance ensures that artifacts introduced by digital sampling or segmentation are minimized and that signal processing techniques can be generalized to any situation.

It is important to note, however, that the overall time varying properties demonstrated by our chosen wavelets were quite small for both decomposition trees. For either tree configuration, we found that the energy contained in a single level of the wavelet decomposition varied by no more than 2.5% when the input signal was shifted. Often times, this value was less than 3%, as shown by the mean values presented in Figures 5 and 6. Hence, the dual-tree system generally improved these properties but such improvements may be of great interest only for applications where time invariant denoising is of critical importance. Real-time applications can utilize the same benefit, but may be willing to accept a greater amount of potential error in order to minimize computation time. In summary, the dual-tree configuration can improve the time invariant properties of a wavelet decomposition of swallowing vibration signals.

4.2 Denoising Effectiveness

Similar to our examination of time varying properties, we found that the denoising effectiveness offered by the dual-tree wavelet decomposition varied somewhat with the specific wavelet. The Daubechies, Coiflet, and Real Matched wavelets were all able to eliminate more of the additive Gaussian white noise from the artificial signal when implemented in the dual-tree configuration. The Artificial Matched wavelet, on the other hand, performed slightly better in the single-tree configuration while the Meyer and Symlet wavelets performed relatively poorly in the dual-tree configuration. The performance of the Symlet, Meyer, and Artificial Matched wavelets offer a common trade-off when implemented in either a single or dual-tree system. The first system offers better denoising properties, while the second provides greater time invariance for these specific wavelets. The remaining wavelets perform better overall in the dual-tree system. Judging by Figures 7 and 8, this discrepancy seems to be related to the symmetry of chosen wavelet, with the more asymmetrical wavelets performing better in the dual-tree configuration. However, this may simply be related to our specific artificial test signal and not the underlying decomposition, and so more research would be necessary to provide a conclusive analysis. Regardless, we see that the dual-tree wavelet decomposition does offer potential advantages with regard to the removal of additive noise from cervical auscultation-like signals.

The benefits of the dual-tree configuration are geared towards high-precision applications. The single-tree system is able to remove at least 80% of the additive noise using any wavelet, and the dual-tree system can remove approximately 5% more for those wavelets that have improved performance. This offers a trade-off between a longer computation time and the removal of more noise, or the removal of slightly less noise in less time.

Our results for the denoising of real signals are similar to what was found with regards to the artificial signal. Again, the Symlet wavelet performed poorly in the dual-tree configuration while the Meyer wavelet performed nearly the same and the remaining wavelets showed varying amounts of improvements. We have observed a maximum increase of approximately 1.5 dB. As with the artificial signal, we see that the dual-tree decomposition offers somewhat greater denoising ability with regards to cervical auscultation signals, but at the cost of greater computational time and complexity. An additional benefit of the dual-tree configuration is the consistency of the results. The amount of noise removed from the real signal was nearly independent of the choice of wavelet when using this method. Furthermore, there was less variance of the algorithm's performance, indicating that the amount of noise removed from each signal was similar. This is likely the result of the final step of the dual-tree system which combines the output of each tree, thereby minimizing the effects of outliers or other significant deviations that occur in a single decomposition tree. The benefits offered by the dual-tree decomposition are still an important consideration in high-precision applications and are worthy of consideration.

4.3 Matched Wavelet Effectiveness

Ultimately, we demonstrated that our Real Matched wavelet does offer certain advantages over existing wavelets. Its time invariant properties and denoising effectiveness with regards to our artificial signal are comparable to the more widely implemented wavelets included in this study. This was true for the typical single tree wavelet decomposition in addition to the less common dual-tree decomposition structure. The performance of our Artificial Matched wavelet in these same tasks provides an upper limit to the usefulness of this wavelet matching technique and demonstrates its potential benefit. However, the goal of this Real Matched wavelet was to provide a more sparse decomposition of swallowing vibrations so as to allow for superior noise removal. In that application, it was successful and was able to remove the greatest amount of noise from our real data. It must be noted, though, that this benefit is very small in magnitude when compared to existing wavelets and comes with a notable drawback. The Daubechies and related wavelet families can be accurately

represented by a very small number of coefficients. This study, for example, used only 6. The Meyer wavelet, and by extension our Real Matched wavelet as they share certain formulation similarities [33], requires an order of magnitude more coefficients to provide a reasonable FIR filter approximation. Similarly, though the amplitude spectrum of our Real Matched wavelet much more closely resembles the amplitude spectrum of a swallowing vibration, it does not share all of the useful properties of the Meyer wavelet such as infinite differentiability or symmetry. Therefore, we conclude that the Real Matched wavelet offers some advantages with respect to the removal of noise from cervical auscultation signals, but with additional computational and analytical overhead.

4.4 Limitations

The findings presented in this study come with a number of notable limitations. First, our experiment tested a finite selection of wavelets. Our matched wavelets were formulated so that their power spectrums most closely matched the power spectrums of our signals of interest. However, this is not the only possible method one can use to design a matched wavelet and it is possible that an alternative method, such as one that incorporates time-domain information, could produce superior results. Likewise, these wavelets were compared to a finite selection of pre-existing wavelet families that were chosen based on their widespread use with swallowing signals rather than their possession of specific mathematical characteristics. While our manuscript provides a broad selection of results as well as valuable insights towards this aspect of cervical auscultation analysis, it is by no means a complete overview of all possibilities. In addition to the limited selection of wavelets tested, our experiment also made certain assumptions about what constitutes a cervical auscultation signal. The beginning and end points of each swallow were based on widely accepted clinical landmarks. However, these points do not necessarily correlate perfectly with the beginning and end of cervical vibrations [34]. While the results presented in this study are valuable when analyzing data from this clinical perspective, it may be beneficial to investigate how these algorithms perform when incorporating data from outside of this accepted range so that information not included in a standard clinical examination may also be studied. Such actions would alter the resulting matched wavelet and produce different effects with regards to the time varying properties of the denoising process. Third, our study did not take into account the computational complexity of wavelet denoising techniques, aside from mentioning that the dual-tree wavelet decomposition is a more efficient way of achieving time invariance than the undecimated transform. There exist several more time-efficient wavelet denoising algorithms that may be able to achieve performance

similar to the dual-tree decomposition but can be computed faster. Future research that may attempt to implement a wavelet denoising step in a practical swallowing analysis system may want to take this aspect into account. Finally, this experiment focused on studying techniques to remove white Gaussian noise from a swallowing signal. This might not be the best approach as there may be other sources of noise that could be of greater concern when recording real physiological signals. However due to the existence of whitening transforms, this approach is the most generalizable and provides a solid point of comparison for more noise reduction techniques that may be more complex or targeted to specific noise sources.

5 Conclusion

In this study, we sought to improve the wavelet denoising methods traditionally implemented with regards to cervical auscultation signals. To that end, we sought to first create a wavelet that was optimized for use with swallowing vibration signals, specifically with regards to its power spectrum, in order to allow for a stricter threshold and greater noise removal when compared to more generalized wavelet families. In addition, we implemented a dual-tree wavelet decomposition in order to correct for the time varying properties introduced with the commonly used single-tree variant. We were able to accomplish both objectives and produced a wavelet denoising technique that provided more noise removal and improved time varying properties. However, we note that these advantages are small in magnitude and that the benefits offered are of most use when attempting to identify weak signal features.

6 Acknowledgements

Research reported in this publication was supported by the Eunice Kennedy Shriver National Institute Of Child Health and Human Development of the National Institutes of Health under Award Number R01HD074819. The content is solely the responsibility of the authors and does not necessarily represent the official views of the National Institutes of Health.

References

[1] M. Spieker, "Evaluating dysphagia," *American Family Physician*, vol. 61, no. 12, pp. 3639–3648, June 2000.

[2] J. Coyle, L. Davis, C. Easterling, D. Graner, S. Langmore, S. Leder, M. Lefton-Greif, P. Leslie, J. Logemann, L. Mackay, B. Martin-Harris, J. Murray, B. Sonies, and C. M. Steele, "Oropharyngeal dysphagia assessment and treatment efficacy: Setting the record straight (response to Campbell-Taylor)," *Journal of the American Medical Directors Association*, vol. 10, no. 1, pp. 62–66, January 2009.

[3] I. Cook and P. Kahrilas, "American gastroenterological association technical review on management of oropharyngeal dysphagia," American Gastroenterological Association, Tech. Rep. 116 (2), January 1999.

[4] M. Rugiu, "Role of videofluoroscopy in evaluation of neurologic dysphagia," *ACTA Otorhinolaryngologica Italica*, vol. 27, no. 6, pp. 306–316, December 2007.

[5] H. Bonilha, K. Humphries, J. Blair, E. Hill, K. McGrattan, and B. Carnes, "Radiation exposure time during mbss: Influence of swallowing impairment severity, medical diagnosis, clinician experience, and standardized protocol use," *Dysphagia*, vol. 28, no. 1, pp. 77–85, 2013.

[6] I. Zammit-Maempel, C. Chapple, and P. Leslie, "Radiation dose in videofluoroscopic swallow studies," *Dysphagia*, vol. 22, no. 1, pp. 13–15, 2006.

[7] A. da Silva, J. L. Neto, and P. Santoro, "Comparison between videofluoroscopy and endoscopic evaluation of swallowing for the diagnosis of dysphagia in children," *Otolaryngology - Head and Neck Surgery*, vol. 143, no. 2, pp. 204–209, 2010.

[8] S. Langmore, K. Schatz, and N. Olsen, "Fiberoptic endoscopic examination of swallowing safety: A new procedure," *Dysphagia*, vol. 2, no. 4, pp. 216–219, 1988.

[9] S. Langmore, K. Schatz, and N. Olson, "Endoscopic and videofluoroscopic evaluations of swallowing and aspiration," *The Annals of Otology, Rhinology, and Laryngology*, vol. 100, no. 8, pp. 678–681, 1991.

[10] B. Martin-Harris, J. Logemann, S. McMahon, M. Schleicher, and J. Sandidge, "Clinical utility of the modified barium swallow," *Dysphagia*, vol. 15, no. 3, pp. 136–141, 2000.

[11] A. Nacci, F. Ursino, R. L. Vela, F. Matteucci, V. Mallardi, and B. Fattori, "Fiberoptic endoscopic evaluation of swallowing (FEES): Proposal for informed consent," *Acta Otorhinolaryngologica Italica: Organo Ufficiale Della Societa Italiana Di Otorinolaringologia E Chirurgia Cervico-Facciale*, vol. 28, no. 3, pp. 206–211, 2008.

[12] J. M. Dudik, J. L. Coyle, and E. Sejdić, "Dysphagia screening: Contributions of cervical auscultation signals and modern signal processing techniques," *IEEE Transactions on Human-Machine Systems*, vol. 45, no. 4, pp. 465–477, August 2015.

[13] P. Leslie, M. Drinnan, P. Finn, G. Ford, and J. Wilson, "Reliability and validity of cervical auscultation: A controlled comparison using videofluoroscopy," *Dysphagia*, vol. 19, no. 4, pp. 231–240, 2004.

[14] P. Zenner, D. Losinski, and R. Mills, "Using cervical auscultation in the clinical dysphagia examination in long-term care," *Dysphagia*, vol. 10, no. 1, pp. 27–31, Janurary 1995.

[15] K. L. Shem, D. Castillo, S. L. Wong, J. Chang, M.-C. Kao, and S. Kolakowsky-Hayner, "Diagnostic accuracy of bedside swallow evaluation versus videofluoroscopy to assess dysphagia in inidividuals with tetraplegia," *PM&R*, vol. 4, no. 4, pp. 283–289, April 2012.

[16] D. Donoho and I. Johnstone, "Ideal spatial adaptation by wavelet shrinkage," *Biometrika*, vol. 81, no. 3, pp. 425–455, 1994.

[17] N. G. Kingsbury, "Complex wavelets for shift invariant analysis and filtering of signals," *Applied and Computational Harmonic Analysis*, vol. 10, no. 3, pp. 234–253, May 2001.

[18] E. Sejdić, C. M. Steele, and T. Chau, "A procedure for denoising of dual-axis swallowing accelerometry signals," *Physiological Measurements*, vol. 31, no. 1, pp. N1–N9, January 2010.

[19] I. Jestrović, J. Dudik, B. Luan, J. Coyle, and E. Sejdić, "The effects of increased fluid viscosity on swallowing sounds in healthy adults," *Biomedical Engineering Online*, vol. 12, no. 90, pp. 1–17, September 2013.

[20] J. M. Dudik, A. Kurosu, J. L. Coyle, and E. Sejdić, "The effects of dysphagia on swallowing sounds and vibrations in adults," *IEEE Transactions on Neural Systems and Rehabilitation Engineering*, 2014, under review.

[21] E. Sejdić, C. M. Steele, and T. Chau, "Segmentation of dual-axis swallowing accelerometry signals in healthy subjects with analysis of anthropometric effects on duration of swallowing activities," *IEEE Transactions of Biomedical Engineering*, vol. 56, no. 4, pp. 1090–1097, April 2009.

[22] K. Takahashi, M. Groher, and K. ichi Michi, "Methodology for detecting swallowing sounds," *Dysphagia*, vol. 9, no. 1, pp. 54–62, January 1994.

[23] J. Lee, E. Sejdić, C. M. Steele, and T. Chau, "Effects of stimuli on dual-axis swallowing accelerometry signals in a healthy population," *Biomedical Engineering Online*, vol. 9, no. 7, pp. 1–14, February 2010.

[24] S. Hamlet, D. Penney, and J. Formolo, "Stethoscope acoustics and cervical auscultation of swallowing," *Dysphagia*, vol. 9, no. 1, pp. 63–68, January 1994.

[25] E. Sejdić, V. Komisar, C. M. Steele, and T. Chau, "Baseline characteristics of dual-axis cervical accelerometry signals," *Annals of Biomedical Engineering*, vol. 38, no. 3, pp. 1048–1059, March 2010.

[26] L. Marple, "A new autoregressive spectrum analysis algorithm," *IEEE Transactions on Acoustics, Speech, and Signal Processing*, vol. ASSP-28, no. 4, pp. 441–454, August 1980.

[27] E. Sejdić, C. M. Steele, and T. Chau, "A method for removal of low frequency components associated with head movements from dual-axis swallowing accelerometry signals," *PLoS ONE*, vol. 7, no. 3, pp. 1–8, March 2012.

[28] E. Sejdić, C. Steele, and T. Chau, "Understanding the statistical persistence of dual-axis swallowing accelerometry signals," *Computers in Biology and Medicine*, vol. 40, no. 11, pp. 839–844, November 2010.

[29] J. M. Dudik, I. Jestrović, B. Luan, J. L. Coyle, and E. Sejdić, "A comparative analysis of swallowing accelerometry and sounds during saliva swallows," *Biomedical Engineering Online*, vol. 14, no. 3, pp. 1–15, January 2015.

[30] M. Nikjoo, C. Steele, E. Sejdić, and T. Chau, "Automatic discrimination between safe and unsafe swallowing using a reputation-based classifier," *Biomedical Engineering Online*, vol. 10, no. 100, pp. 1–17, November 2011.

[31] C. Merey, A. Kushki, E. Sejdić, G. Berall, and T. Chau, "Quantitative classification of pediatric swallowing through accelerometry," *Journal of NeuroEngineering and Rehabilitation*, vol. 9, no. 34, pp. 1–8, June 2012.

[32] C. Steele, E. Sejdić, and T. Chau, "Noninvasive detection of thin-liquid aspiration using dual-axis swallowing accelerometry," *Dysphagia*, vol. 28, no. 1, pp. 105–112, March 2013.

[33] J. O. Chapa and R. M. Rao, "Algorithms for designing wavelets to match a specified signal," *IEEE Transactions on Signal Processing*, vol. 48, no. 12, pp. 3395–3406, December 2000.

[34] J. M. Dudik, A. Kurosu, J. L. Coyle, and E. Sejdić, "A comparative analysis of DBSCAN, k-means, and quadratic variation algorithms for for automatic identification of swallows from swallowing accelerometry signals," *Computers in Biology and Medicine*, vol. 59, no. 1, pp. 10–18, April 2015.